2018 18th European Conference on Radiation and Its Effects on Components and Systems (RADECS) | 978-1-7281-0216-0/18/$31.00 ©2018 IEEE | DOI: 10.1109/RADECS45761.2018.9328700

Single-Event Transients in a PIN Photodiode and a Single-Photon Avalanche Diode Integrated in 0.35µm CMOS

Michael Hofbauer, *Member, IEEE,* Bernhard Steindl, Kerstin Schneider-Hornstein, Bernhard Goll, *Member, IEEE,* Kay-Obbe Voss, and Horst Zimmermann, *Senior Member, IEEE*

***Abstract*—Single-event transients (SETs) in a PIN photodiode and a single-photon avalanche diode (SPAD), both fabricated in the same 0.35µm CMOS process, are compared under heavy ion irradiation. The experimental results suggest that mainly the low-doped epitaxial layer defines the amount of collected charge. High current peaks at the output of the photodetectors, necessitate precautions in the quencher and read-out circuit design.**

***Index Terms*— single-event transient (SET), PIN photodiode, single-photon avalanche diode (SPAD), avalanche photo diode (APD), heavy ions, micro-beam, CMOS.**

I. Introduction

INTEGRATED optical detectors, such as PIN photodiodes, avalanche photodiodes (APDs), and single photon avalanche diodes (SPADs) are important components in countless applications. They are used for optical data communication, sensing applications, and many more.

PIN photodiodes are very efficient photodetectors with quantum efficiencies close to 100%. APDs additionally have an internal gain, especially useful for low light applications. SPADs are APDs operated above their breakdown voltage, therefore triggering self-sustained avalanches if a photon is absorbed. They allow single photon detection, as their name already suggests. As soon as an avalanche is triggered, it needs to be stopped again. This is done by reducing the reverse voltage on the SPAD below its breakdown voltage. This can be done actively by a dedicated active quenching circuit (AQC), or passively, typically by a simple series resistor. In the time period from triggering the avalanche until restoring the reverse voltage after quenching it below the breakdown voltage, the SPAD is blind and the corresponding time period is called dead time. AQCs typically are much faster than passive quenching (i.e. their dead time is shorter), but they require more chip area. The photon detection efficiency (PDE) of SPADs can reach 75% if fabricated in specialized processes [1]. The SPAD investigated in this work is fabricated in a pin-photodiode 0.35µm CMOS process. This allows integrating the detector with additional circuitry such as active quenching circuits. The PDE of a comparable SPAD in the same technology reaches values exceeding 40% using an AQC, depending on the wavelength of the photon [2]. It should be possible to improve this value in future by improving the quenching circuit.

Since SPADs are capable of detecting single photons and can be integrated, they started to be used in many applications, such as positron emission tomography (PET), fluorescence microscopy, and quantum cryptography.

Quantum cryptography is a fast emerging field, allowing secure transmission of data. Commercial hardware for quantum key distribution (QKD) is already available. Currently, secure links using optical fibers are limited to a few hundred kilometers, because of absorption. To overcome this distance limitation, QKD networks using satellite links are being tested [3]. These satellites require single photon detectors. It is therefore very important to investigate radiation effects in these type of optical detectors. Since SPADs are operated above their breakdown voltage, high amplitude current peaks can be expected after being hit by an ionizing particle.

For CMOS image sensors, valuable experimental results concerning single event transients are already available, e.g. in [4]-[6]. In these types of sensors, not only SETs affecting the photodiodes were investigated, but also the effects on the other circuits integrated on the same chip. Additionally, effects such as single event latch-up (SEL) were investigated [6], since some types of CMOS images sensors seem to be prone to this effect. However, all these experiments were focused on sensors containing standard photodiodes without internal gain.

In [7] device degradation of a Si APD under heavy ion and gamma irradiation was investigated. In [8] charge collection mechanisms in InP-InGaAs APDs under heavy ion irradiation were studied. In their device the authors see a significant increase of the collected charge due to avalanche multiplication.

In this paper, we compare the single event transient (SET) response of a PIN photodiode and a SPAD on heavy ion hits

The authors acknowledge financial support from the Austrian Science Fund (FWF) under grant no. [P28335-N30].

M. Hofbauer, B. Steindl, K. Schneider-Hornstein, B. Goll, and H. Zimmermann are with the Institute of Electrodynamics, Microwave and Circuit Engineering, Vienna University of Technology, 1040 Vienna, Austria (e-mail: michael.hofbauer@tuwien.ac.at, bernhard.steindl@tuwien.ac.at, kerstin.schneider-hornstein@tuwien.ac.at, bernhard.goll@tuwien.ac.at, horst.zimmermann@tuwien.ac.at).

K.-O.Voss is with the GSI Helmholtzzentrum für Schwerionenforschung GmbH, 64291 Darmstadt, Germany (e-mail: K.-O.Voss@gsi.de).

(^{197}Au with a linear energy transfer of approximately 97 MeVcm²/mg), to investigate the differences in the charge collection process. Both detectors were fabricated in the same 0.35 µm CMOS technology. The SPAD can be operated in linear mode or in Geiger mode.

II. PIN Photodiode and SPAD Design

The PIN photodiode and the SPAD were designed in a 0.35 µm pin-photodiode CMOS process. In this process, a substrate with a low-doped epitaxial layer (p-epi) is used, to improve the responsivity of the PIN photodiode and the PDE of the SPAD, especially for longer wavelengths (i.e. 700 nm-1000 nm). The structure of the PIN photodiode is depicted in Fig. 1. Its active diameter is 80 µm. The cathode is formed by a highly doped n++ region. The substrate is contacted by a p++ contact region surrounding the n++ cathode. The thickness of the epitaxial layer is approximately 12 µm. It is fully depleted even for very small reverse voltages across the PIN photodiode, due to the low doping concentration in this layer. In Fig. 1 the border of the depletion region is indicated by dashed lines. The breakdown voltage is approximately 120V. The PIN photodiode has an opto window, which means that the oxide thickness above the active area is strongly reduced to decrease interference effects in the oxide stack.

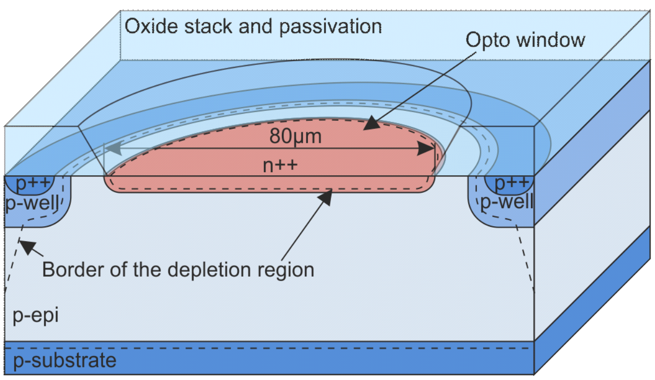

Fig. 1 Structure of the investigated PIN photodiode (not to scale).

The structure of the SPAD is quite similar to the structure of the PIN photodiode, as depicted in Fig. 2. There is an additional p-well, forming the multiplication zone together with the n++ zone. In this multiplication zone, for a large enough reverse voltage V_r, impact ionization by the photo-generated charges can result in a gain in the photocurrent. In linear mode the diodes works as an APD and the gain increases with increasing reverse voltage and can reach values larger than 1000.

When the reverse voltage is further increased above the breakdown voltage, the diode operates in Geiger mode. In this mode, the gain can reach a value of several millions and is mainly defined by the quenching approach and V_r. Please note, contrary to the PIN photodiode, the SPAD does not have an opto window, resulting in ripples in the spectral PDE as shown in [2] for a similar device. The breakdown voltage of the investigated SPAD was approximately 32 V. For a full depletion of the p-well and the p-epi region below the active area, the reverse voltage needs to exceed approximately 20 V. The thickness of the oxide stack including the passivation is 8 µm - 9 µm.

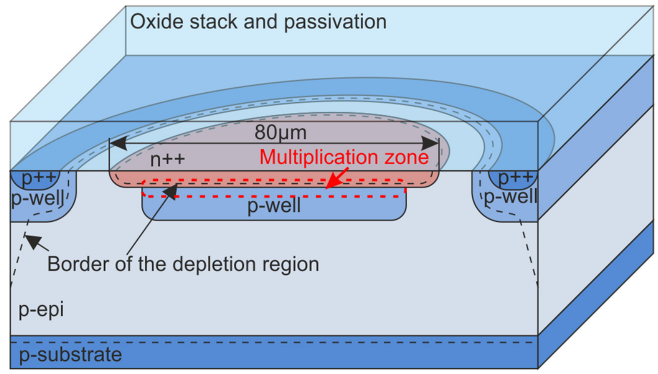

Fig. 2 Structure of the investigated SPAD (not to scale).

III. Experimental Setup

The experiments were conducted at the micro-beam facility at GSI in Darmstadt, Germany, using a focused ion beam consisting of ^{197}Au ions with an energy of 4.8 MeV per atomic mass unit, resulting in a linear energy transfer at the silicon surface of approximately 97 MeV·cm²/mg. The oxide stack of the SPAD has only minor influence on the LET on the silicon surface.

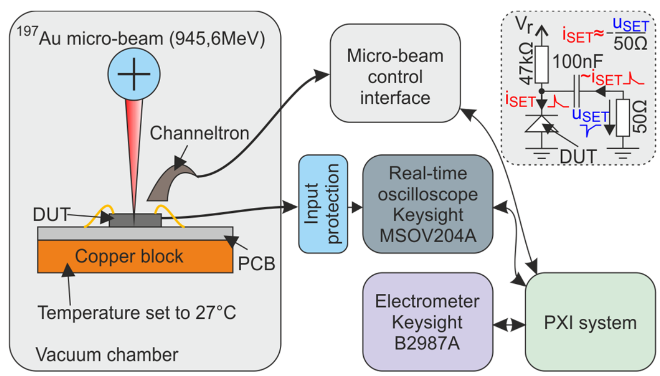

Fig. 3 Measurement setup and simplified equivalent circuit (in the dashed box).

The measurement system is depicted in Fig. 3. It mainly consists of the device under test (DUT), namely the PIN photodiode or the SPAD, the micro-beam instrument, an electrometer as power supply for the DUTs (Keysight B2987A), a fast real-time oscilloscope (Keysight MSOV204A) with an analog bandwidth of 20GHz for recording the SETs, and a PXI system (Peripheral Component Interconnect (PCI) eXtensions for Instrumentation) from National Instruments for interfacing the micro-beam's control system and for controlling the experiment.

The DUTs were bonded onto a printed circuit board (PCB) with an RF substrate (Rogers RO4350). The PCB was mounted onto a copper block inside a vacuum chamber. The temperature of the copper block and therefore also of the DUT was controlled by a thermo-electric cooler and was set to 27°C. Both, the SPAD and the PIN photodiode had a 47 kΩ resistor connected in series. For the SPAD this resistor was used as passive quenching resistor. The output of this circuit was connected to the input of the fast real-time oscilloscope using high performance RF cables. In order to protect the sensitive inputs of the oscilloscope, the signal was ac coupled. Additionally, input protection was used to protect the real-time oscilloscope. To increase the usable voltage range for the SPAD experiment a 6 dB attenuator was inserted before the input protection. This additional attenuation was corrected in all the results shown in the next section. Since the value of the series resistor is much higher than the input resistance of the oscilloscope (50Ω), almost the complete current pulse delivered by the DUT under irradiation flows through the oscilloscope and the voltage transient u_{set} can be measured. Because of this, the transient SET current pulse i_{set} can be approximated by

$$i_{set} \approx -\frac{u_{set}}{50\Omega}, \tag{1}$$

as shown in Fig. 3 in the dashed region.

The ion-beam delivered by a linear accelerator, is focused by means of micro-slits and a magnetic lens. The achievable spot size is in the range of 500 nm. Using magnetic beam deflection, the ion beam can be scanned over the chip surface. Because of this, it is possible to investigate how different regions of the optical detectors respond to an ion hit. It is possible to accurately distinguish between hits of the active area and its border. During the experiment the micro-beam was scanned over the optical detectors with a step size of 2 µm. A fast electrostatic beam switch allows turning on and off the micro-beam within nano seconds. Close to the chip's surface, a channeltron is mounted. This channeltron detects electrons emitted by the chip surface after an ion hit, allowing to generate a trigger signal that indicates that the chip was hit by an ion.

The PXI system was controlling the experiment. The trigger from the channeltron triggered the oscilloscope to store the transients at the output of the DUT after each ion hit. Additionally, the beam was turned off after each trigger signal before steering the beam to the next position in order to guarantee that only one ion at a time hits the DUT.

IV. Results and Discussion

During the measurements, the surface of the DUTs was scanned with the ion beam. For each position, the output of the DUTs was recorded. In Fig. 4 and 5 the extracted current pulse height, full width at half maximum (fwhm) pulse width and the collected charge are shown for each ion hit position and for four different reverse voltages in scatter plots for the PIN photodiode and the SPAD, respectively. Each dot in the scatter plot corresponds to one ion hit. Its location shows the hit location and its color indicates the value of the extracted parameter.

For the PIN photodiode the collected charge is almost independent from the reverse voltage and reaches approximately 18 pC for some of the ion hits in the active area. This can be explained since the low doped epitaxial layer depletes already for a very low reverse voltage, generating a large volume that collects charge. According to SRIM (Stopping and Range of Ions in Matter) [9], for 12µm ion track, corresponding to the thickness of the epitaxial layer, the collected charge should be in the range of 12 pC. However, the recorded transients indicate that some of the charge is collected by a slower diffusion process and might therefore originate from the substrate. Additionally, funneling may play a role [10].

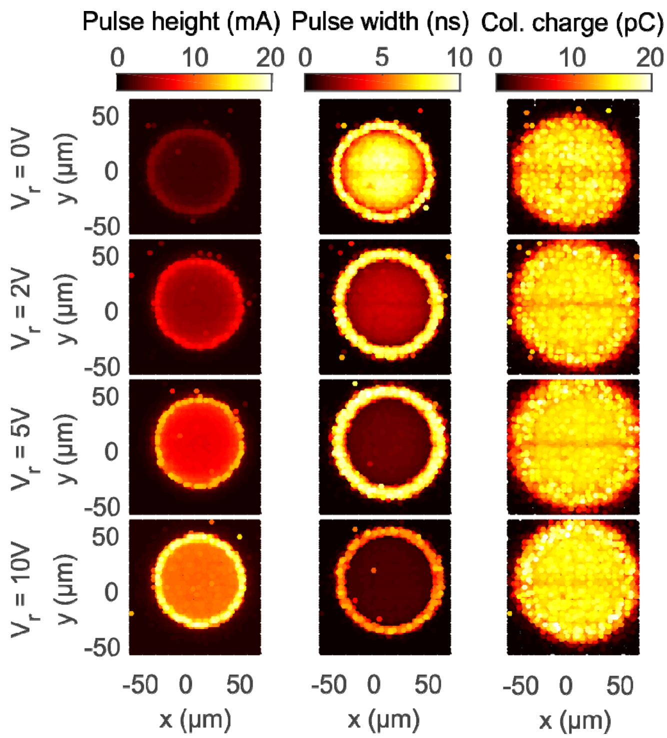

Fig. 4 SET pulse heights (left column), full width at half maximum (fwhm) pulse widths (middle column) and collected charge (right column) at the output of the PIN photodiode, depending on the ion hit position for four different reverse voltages V_r.

For the SPAD the charge collection is smaller for low reverse voltages, because the p-well needs to be depleted, before the epitaxial layer depletes. For large reverse voltages slightly above the breakdown voltage, the charge collection even exceeds 20pC. However, the total charge is in average only approximately 20% higher than for the PIN photodiode. This suggests that avalanche multiplication is not a significant factor for hits with ions with a large LET in the investigated technology. We believe, this can be explained by the local collapse of the electric field in the ion track through the SPAD due to the large amount of deposited charge. This suggests that the large charge collection volume (i.e. predominately the depleted volume) mainly defines the total amount of collected charge. Consequently, in the investigated technology, the collected charge is similar for PIN photodiodes, APDs, and SPADs, since the volume of the depleted region is mainly defined by the thickness of the epitaxial layer.

The pulse heights for the PIN photodiode reaches its maximum at the border of the active area, since the electric field is highest there, due to edge effects. The pulse widths for these highest SETs are very short. However if an ion hits the diode only a little bit further outside of the active area, the pulse width is increasing quickly.

Contrary to the high SETs at the edge of the active area for the PIN photodiode, the maximum pulse height for the SPAD is reached in the center of the active area at a large reverse voltage, since the electric field is largest in the multiplication zone.

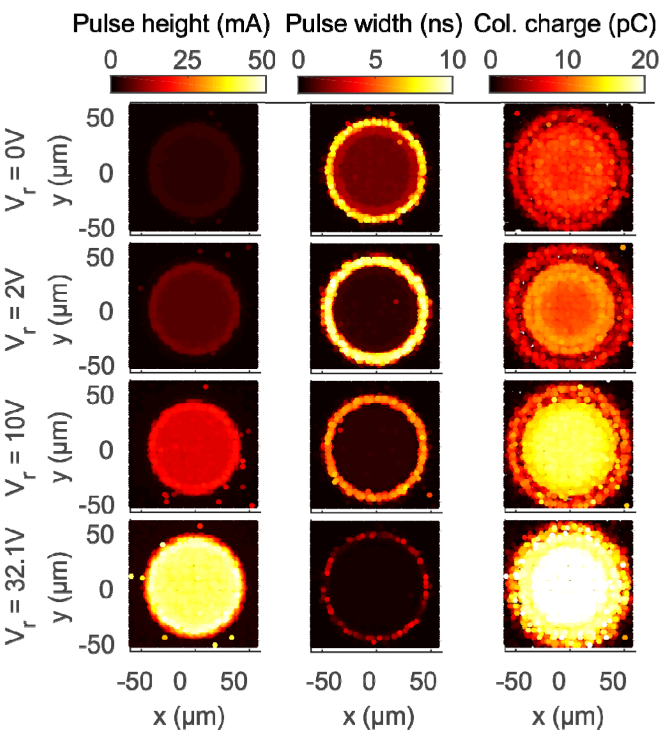

Fig. 5 SET pulse heights (left column), full width at half maximum (fwhm) pulse widths (middle column) and collected charge (right column) at the output of the SPAD, depending on the ion hit position for four different reverse voltages V_r.

The pulse widths are largest in the region surrounding the PIN photodiode and the SPAD. In this region, the diffusion part of the SET increases and the drift part decreases, resulting in a wider effective pulse width.

Fig. 6 and Fig. 7 show scatter plots of the pulse width depending on the pulse heights for four different reverse voltages V_r for the PIN photodiode and the SPAD, respectively. The brightness (or color) of the dots represents V_r. Additionally, the function

$$Pulse\_width = 11ns \cdot mA \cdot \frac{1}{Pulse\_height} \qquad (2)$$

is plotted as a solid line. This function envelopes the point cloud in the scatter plot for the PIN photodiode as well as in the scatter plot for the SPAD. Both devices collect very similar amounts of charge after an ion hit. This collected charge is approximately proportional to the product of the pulse width and the corresponding pulse height.

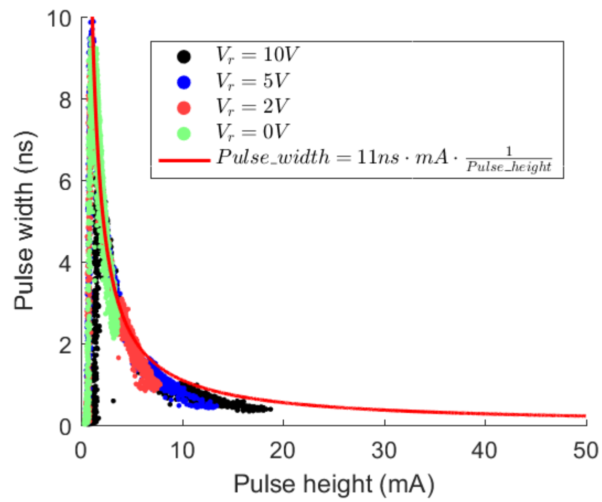

Fig. 6 SET pulse widths versus pulse heights at the output of the PIN photodiode for four different reverse voltages V_r and a function approximating the envelope of the point cloud for comparison with Fig. 7.

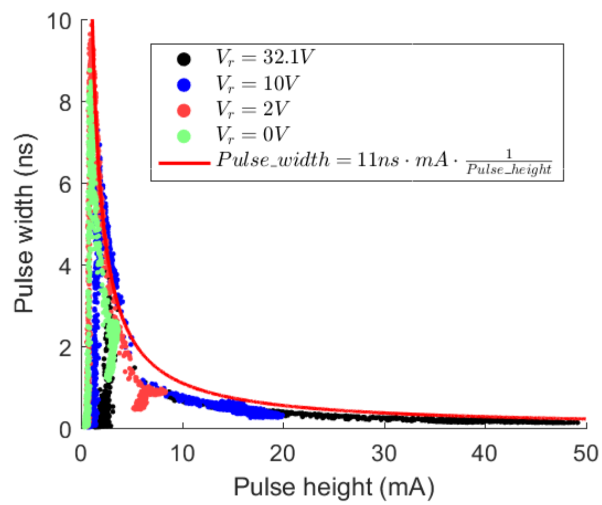

Fig. 7 SET pulse widths versus pulse heights at the output of the SPAD for four different reverse voltages V_r and a function approximating the envelope of the point cloud for comparison with Fig. 6.

Please note, for the measurements for the SPAD at a reverse voltage of 32.1 V the measured pulses exceeding a pulse height of 40mA were slightly distorted due to the input protection of the oscilloscope.

The potentially large current peaks at the output of photodetectors with a thick epitaxial layer under irradiation need to be considered in the design of the quenching and read-out circuitry. The corresponding voltage pulse is limited only by the value of the reverse voltage and therefore may reach tens of volts. This might permanently destroy the integrated circuit. Due to the similar amount of collected charge, this is not only important for the SPAD, but also for APDs and PIN photodiodes if their reverse voltage is large. Typically, the reverse voltage is the largest for SPADs.

V. Conclusion

The comparison of two photodetectors, namely a PIN photodiode and a single photon avalanche diode (SPAD) under heavy ion irradiation (^{197}Au, 945.6 MeV), fabricated in the same technology, revealed that the total collected charge mainly is determined by the thick epitaxial layer and is therefore similar for both detectors, although the SPAD has a very high inherent gain. Consequently, also the relation between pulse width and pulse height for the SETs follows similar rules in both detectors.

The thick epitaxial layer improves photon detection efficiencies. However, it also makes these photodetectors very efficient collectors of charge, deposited within the device after an ion hit. Especially for very high reverse voltages, the charge gets collected fast, resulting in short but high current pulses. SPADs need to be operated at very high reverse voltages, consequently high current pulse amplitudes can be expected when hit by a heavy ion. This needs to be considered when designing quenching and receiver circuits containing SPADs, if radiation effects can be expected.

Acknowledgment

The authors would like to thank Reinhard Lang for preparing the mechanical parts of the measurement setup, and Austrian's Federal Ministry of Science, Research and Economy for covering the travelling costs and our registration fee for this conference within the granted "Exzellenzstipendium".

References

[1] X. Michalet, A. Ingargiola, R.A. Colyer, G. Scalia, S. Weiss, P. Maccagnani, A. Gulinatti, I. Rech, and M. Ghioni, "Silicon photon-counting avalanche diodes for single-molecule fluorescence spectroscopy," *IEEE Journal of Selected Topics in Quantum Electronics*, vol. 20, no. 6, Article ID 3804420, 2014.

[2] H. Zimmermann, B. Steindl, M. Hofbauer, and R. Enne, "Integrated optical fiber receiver reducing the gap to the quantum limit," *Scientific Reports*, vol. 7, Article ID 2652, 2017

[3] S.-K. Liao, W.-Q. Cai, W.-Y. Liu, L. Zhang, Y. Li, J.-G. Ren, J. Yin, Q. Shen, Y. Cao, Z.-P. Li, F.-Z. Li, X.-W. Chen, L.-H. Sun, J.-J. Jia, J.-C. Wu, X.-J. Jiang, J.-F. Wang, Y.-M. Huang, Q. Wang, Y.-L. Zhou, L. Deng, T. Xi, L. Ma, T. Hu, Q. Zhang, Y.-A. Chen, N.-L. Liu, X.-B. Wang, Z.-C. Zhu, C.-Y. Lu, R. Shu, C.-Z. Peng, J.-Y. Wang and J.-W. Pan, "Satellite-to-ground quantum key distribution" in Nature, vol. 549, pp. 43-47, doi: 10.1038/nature23655, 2017

[4] V. Lalucaa, V. Goiffon, P. Magnan, G. Rolland, and S. Petit, "Single-Event effects in CMOS image sensors," IEEE Trans. Nucl. Sci., vol. 60, no. 4, pp. 2494–2502, Aug. 2013

[5] M. Beaumel, D. Hervé, D. Van Aken, P. Pourrouquet, and M. Poizat, "Proton, electron and heavy ion single event effects on the HAS2 CMOS image sensor," in Proc. 14th Eur. Conf. Radiation and its Effects on Component and Systems (RADECS), Oxford, U.K., 2013, article no. PI-4L

[6] C. Virmontois, A. Toulemont, G. Rolland, A. Materne, V. Lalucaa, V. Goiffon, C. Codreanu, C. Durnez, and A. Bardoux, "Radiation-Induced Dose and Single Event Effects in Digital CMOS Image Sensors," *IEEE Transactions on Nuclear Science*, vol. 61, no. 6, pp. 3331 – 3339, 2014

[7] J.S. Laird, S. Onoda, T. Hirao, H. Becker. A. Johnston, and H. Itow, "Effects of gamma and heavy ion damage on the impulse response and pulsed gain of a low breakdown voltage Si avalanche photodiode," *IEEE Transactions on Nuclear Science*, vol. 53, no. 6, pp. 3786 – 3793, 2006

[8] J.S. Laird, T. Hirao, S. Onoda, H. Ohyama, T. Kamiya, "Heavy-ion induced single-event transients in high-speed InP-InGaAs avalanche photodiodes," *IEEE Transactions on Nuclear Science*, vol. 50, no. 6, pp. 2225 – 2232, 2003

[9] J.F. Ziegler, M. D. Ziegler, and J. P. Biersack, "SRIM – The stopping and range of ions in matter (2010)," *Nuclear Instruments and Methods in Physics Research B*, vol. 268, no. 11-12, pp. 1818–1823 2010.

[10] C.M. Hsieh, P.C. Murley and R.R. O'Brien, "A field-funneling effect on the collection of alpha-particle-generated carriers in silicon devices," IEEE Electron Device Letters, vol. 2, no. 4, pp. 103–105, 1981